

Robust Estimation of Similarity Transformation for Visual Object Tracking with Correlation Filters

Yang Li¹, Jianke Zhu^{1,3}, Wenjie Song¹, Zhefeng Wang¹, Hantang Liu¹, Steven C.H. Hoi²

¹College of Computer Science and Technology, Zhejiang University, Hangzhou, China

²School of Information Systems, Singapore Management University, Singapore

³Alibaba-Zhejiang University Joint Research Institute of Frontier Technologies

{liyang89, jkzhu, seeyou, wangzhefeng, liuhantang}@zju.edu.cn, chhoi@smu.edu.sg

Abstract

Most of existing correlation filter-based tracking approaches only estimate simple axis-aligned bounding boxes, and very few of them is capable of recovering the underlying similarity transformation. To a large extent, such limitation restricts the applications of such trackers for a wide range of scenarios. In this paper, we propose a novel correlation filter-based tracker with robust estimation of similarity transformation on the large displacements to tackle this challenging problem. In order to efficiently search in such a large 4-DoF space in real-time, we formulate the problem into two 2-DoF sub-problems and apply an efficient Block Coordinates Descent solver to optimize the estimation result. Specifically, we employ an efficient phase correlation scheme to deal with both scale and rotation changes simultaneously in log-polar coordinates. Moreover, a fast variant of correlation filter is used to predict the translational motion individually. Our experimental results demonstrate that the proposed tracker achieves very promising prediction performance compared with the state-of-the-art visual object tracking methods while still retaining the advantages of efficiency and simplicity in conventional correlation filter-based tracking methods.

1. Introduction

Visual object tracking is one of the fundamental problems in computer vision with a variety of real-world applications, such as video surveillance and robotics. It aims to label the visual object in video sequence given the known bounding box in the first frame. Although having achieved substantial progress during past decade, it is still difficult to deal with the challenging unconstrained environmental variations, such as illumination changes, partial occlusions, motion blur, fast motion and scale variations.

Recently, correlation filter-based methods have attracted



Figure 1: Our proposed method is able to deal with various real-world video sequences more accurately and robustly by taking advantage of the similarity geometric transformation parameterization.

continuous research attention [12, 7, 25, 10] due to its superior performance and robustness in contrast to traditional tracking approaches. Meanwhile, as there is neither pre-training process nor GPU hardware requirement, it maintains simplicity and efficiency compared with deep learning-based methods [20, 26, 14].

However, most of existing correlation filter-based tracking approaches [15, 7, 10, 9, 18] attempt to locate the 2D bounding box of visual object precisely. With correlation

Table 1: Comparison with different kinds of trackers.

Type	Trackers	Sample Num.	Scale	Rot.	Pretrain	Performance	GPU	Speed(fps)
Traditional Methods	Lucas-Kanade based [1]	Depends	✓	✓	×	Fair	×	Depends
	Keypoint based [27]	Depends	✓	✓	×	Fair	×	1~20
	Particle Filter based [31, 16]	300~600	✓	✓	×	Fair	×	1~20
Deep Learning	MDNet [26]	250	✓	×	✓	Excellent	✓	~1
	SiamFC [3]	5	✓	×	✓	Excellent	✓	15~25
Correlation Filter	original CF [15, 5]	1	×	×	×	Fair	×	300+
	DSST [8],SAMF [22]	7~33	✓	×	×	Good	×	20~80
	ECO [7]	17	✓	×	✓	Excellent	✓	6~10
	STECFNR (Ours)	2	✓	×	×	Excellent	×	~140
	STECF (Ours)	2~8	✓	✓	×	Excellent	×	20~30

filters, little attention has been paid on how to efficiently and precisely estimate scale and rotation changes, which are typically represented in a 4-Degree of Freedom (DoF) similarity transformation. To deal with scale changes of the conventional correlation filter-based trackers, Danelljan *et al.* [8] and Li *et al.* [22] extended the 2-DoF representation of original correlation filter-based methods to 3-DoF space, which handles scale changes in object appearance by introducing a pyramid-like scale sampling ensemble. With an extra dimension in geometric representation, the tracking accuracy and robustness are drastically improved. Unfortunately, all these methods have to intensively resample the image in order to estimate the geometric transformation, which incurs huge amounts of computational costs. In addition, their accuracy is limited to the pre-defined dense sampling of the scale pool. This makes them unable to handle the large displacement that is out of the pre-defined range in the status space. Thus, none of these methods is guaranteed to the optimum of the scale estimation. On the other hand, rotation estimation for the correlation filter-based methods has not been fully exploited yet, since it is very easy to drift away from the inaccurate rotation predictions. This greatly limits their scope of applications in various wide situations. Table. 1 summarizes the representative properties of several typical trackers.

To address the above limitations, in this paper, we propose a novel visual object tracker to estimate the similarity transformation of the target efficiently and robustly. Unlike existing correlation filter-based trackers, we formulate the visual object tracking into a status space searching problem in a 4-DoF status space, which gives a more appropriate geometric transformation parameterization for the target. As shown in Fig. 1, the representation in similarity transformation describes the object more correctly and helps to track the visual object more accurately. To yield real-time tracking performance in the 4-DoF space, we propose to tackle the optimization task of estimating the similarity transformation by applying an efficient Block Coordinates Descent (BCD) solver. Specifically, we employ an efficient phase correlation scheme to deal with both scale and rotation changes simultaneously in log-polar coordinates and utilize a fast variant of correlation filter to predict the translational

motion. This scheme sets our approach free from intensive sampling, and greatly boosts the performance in the 4-DoF space. More importantly, as BCD searches the entire similarity transformation space, the proposed tracker achieves very accurate prediction performance in large displacement motion while still retaining advantages of the efficiency and simplicity in conventional correlation filter. Experimental results demonstrate that our approach is not only robust and accurate for both generic object and planar object tracking but also very computationally efficient compared with the state-of-the-art visual object tracking methods.

2. Related Work

In visual object tracking community, scale and rotation estimation has been investigated for decades. Traditionally, there are three genres to deal with scale and rotation changes. The most widely used approach is to iteratively search in an affine status space with gradient descent-based method [1, 32]. However, they are easy to get stuck at local optima, which are not robust for large displacements. Trackers based on particle filter framework [31, 16, 39] search the status space stochastically by observing the samples, which are employed to estimate the global optima in the status space. Their results are highly related to the motion model that controls the distribution of the 6-DoF transformation. This makes the tracker perform inconsistently in different situations. Another choice is to take advantage of keypoint matching to predict the geometric transformation [27, 24, 41]. These keypoint-based trackers first detect feature points on the object, and then find the matched points in the following frames. Naturally, they can handle any kind of transformations with the matched feature points. Due to the lack of global information on the whole target, these trackers cannot effectively handle the general objects [19].

Our proposed method is highly related to correlation filter-based trackers [15, 5]. DSST [8] and SAMF [22] extend the original correlation filter to adapt the scale changes in the sequences. Staple [2] combines color information with correlation filter method in order to build a robust and efficient tracker. Later, SRDCF [9] and BACF [12] decou-

ple the relationship between the size of filter and searching range. These approaches enable the correlation filter-based methods to have larger searching range while maintaining a relative compact presentation of the learned filters. CACF [25] learns the filter with the additional negative samples to enhance the robustness. Note that all these approaches emphasize on the efficacy issue, which employs either DSST or SAMF to deal with the scale changes. However, the scale estimation becomes less reliable when the scale variation is larger than the predefined scale in the searching pool. More importantly, these methods cannot deal with rotation changes. In contrast to the conventional methods, our proposed work extends the capability of correlation filter from translation-scale estimation to the full 2D similarity transformation, which is able to handle the large displacement by finding an optimal status space.

Recently, deep learning-based methods achieve very impressive performance [26, 3, 13, 37]. MDNet [26] leverages the advantage of massive sequences to learn an end-to-end neural network for visual object tracking. SiameseFC [3] aims to match the template and the following frame with a fully-convolutional Siamese network trained end-to-end. Moreover, CCOT [10] improves the tracking performance by integrating the powerful convolutional neural network (CNN) feature into the correlation filter framework and ECO [7] presents a more efficient approach. Meanwhile, CFNet [34] manage to reformulate the correlation filter-based problem under neural networks framework. CREST [33] further combines residual learning with correlation filter into neural networks to improve the performance.

Fourier Mellin image registration and its variants [6, 29, 40] are also highly related to our proposed approach. These methods usually convert both the test image and template into log-polar coordinates, in which the relative scale and rotation changes turn into the translational displacement. Thus, the phase correlation between these two images gives the estimation of relative scale and rotation changes. Ravichandran and Casasent [29] propose a rotation-invariant correlation filter to detect the same object in the polar coordinates from a god view. Zokai and Wolberg [40] propose an image registration method to recover large-scale similarity with log-polar coordinates in spatial domain. Recently, Li *et al.* [21] and Zhang *et al.* [38] introduce the log-polar coordinates into correlation filter-based method to estimate the rotation and scale. Instead of learning another correlation filter for scale-rotation estimation, we directly employ phase correlation operation in log-polar coordinates. Moreover, we propose an efficient Block Coordinates Descent optimization scheme to estimate translation and scale-rotation alternatively, which is able to deal with large displacement motions with real-time performance.

3. Our Approach

In this paper, we propose a novel tracking approach to enable the tracker with 2D similarity transformation estimation capability. To this end, we follow the track-by-detection paradigm to formulate our method.

3.1. Robust Estimation of Similarity Transformation

Given an image patch \mathbf{x}_i sampled from the i -th frame I_i in a video sequence, the key idea of our proposed approach is to estimate the similarity transformation $Sim(2)$ in 2D image space of the tracked target. To this end, we need to predict a 4-DoF transformation status vector $\tau_i \in \mathcal{R}^4$ based on the output of the previous frame. Generally, τ_i is obtained by optimizing the following score function:

$$\tau_i = \arg \max_{\tau \in Sim(2)} f(\mathcal{W}(I_i, \tau); \mathbf{h}_{i-1}), \quad (1)$$

where $f(\cdot)$ is a score function with the model \mathbf{h}_{i-1} learned from the previous frames $I_{1:i-1}$. \mathcal{W} is an image warping function that samples the image I_i with respect to the similarity transformation status vector τ .

The 2D similarity transformation $Sim(2)$ deals with 4-DoF $\{t_x, t_y, \theta, s\}$ motion, where $\{t_x, t_y\}$ denotes the 2D translation. θ denotes the in-plane rotation angle, and s represents the scale change with respect to the template. Obviously, $Sim(2)$ has a quite large searching space, which is especially challenging for real-time applications. A typical remedy is to make use of effective sampling techniques to greatly reduce the searching space [11].

Since the tracking model \mathbf{h}_{i-1} is learned from the previous frame, which is kept constant during the prediction. Thus, the score function f is only related to the status vector τ . We abuse the notation for simplicity:

$$f_i(\tau) = f(\mathcal{W}(I_i, \tau); \mathbf{h}_{i-1}). \quad (2)$$

Typically, most of the conventional correlation filter-based methods only take into account of in-plane translation with 2-DoF, where the score function f_i can be calculated completely and efficiently by taking advantage of Convolution Theorem. To search the 4-DoF similarity space, the total number of candidate status exponentially increases.

Although Eq. 1 is usually non-convex, the optimal translation is near to the one in the previous frame in object tracking scenarios. Thus, we assume that the function is convex and smooth in the nearby region, and split the similarity transformation $Sim(2)$ into two blocks, $\mathbf{t} = \{t_x, t_y\}$ and $\rho = \{\theta, s\}$, respectively. We propose a score function $f_i(\tau)$, which is the linear combination of two separate ones:

$$f_i(\tau; \mathbf{h}_{i-1}) = \eta f_t(\mathbf{t}; \mathbf{h}_t) + (1 - \eta) f_\rho(\rho; \mathbf{h}_\rho), \quad (3)$$

where η is an interpolation coefficient. f_t is the translational score function, and f_ρ denotes the scale and rotation score

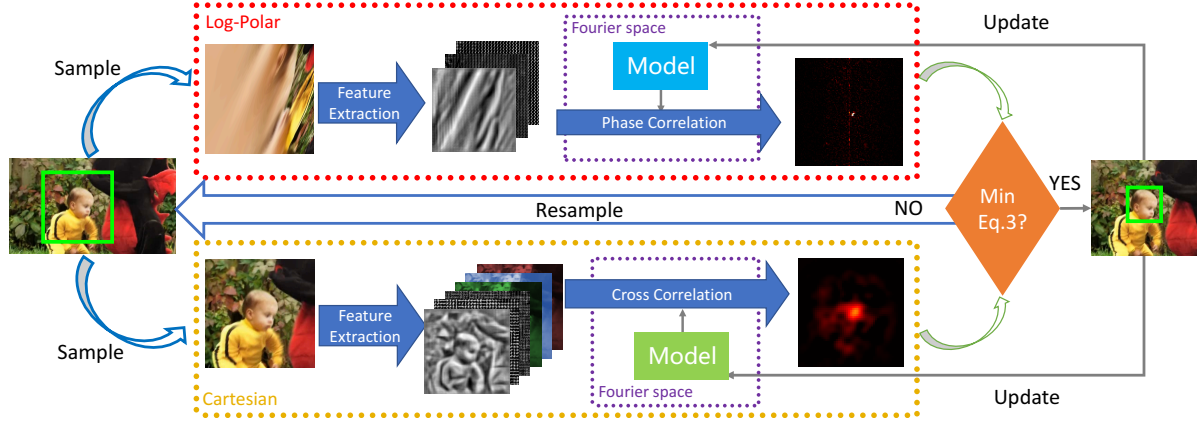


Figure 2: Overview of our proposed approach.

function. Please note that we omit the subscript $i - 1$ of \mathbf{h}_t and \mathbf{h}_ρ for simplicity.

According to the Block Coordinate Descent Methods [30, 28], we optimize the following two subproblems alternatively to achieve the global solution:

$$\arg \max_{\mathbf{t}} f_i(\mathbf{t}, \rho^*) = \arg \max_{\mathbf{t}} f_t(\mathbf{t}) \quad (4)$$

$$\arg \max_{\rho} f_i(\mathbf{t}^*, \rho) = \arg \max_{\rho} f_\rho(\rho), \quad (5)$$

where ρ^* and \mathbf{t}^* denote the local optimal estimation result from previous iteration, which is fixed for the current subproblem. Thus, the key to solving Eq. 1 in real-time is to find the efficient solvers for the above two subproblems.

3.2. Translation Estimation by Correlation Filter

Translation vector \mathbf{t} can be effectively estimated by Discriminative Correlation Filters (DCF) [15, 17]. A large part of its success is mainly due to the Fourier trick and translation-equivariance within a certain range, which calculates the f_t in the spatial space exactly. According to the property of DCF, the following equation can be obtained:

$$f_t(\mathcal{W}(I, \mathbf{t}); \mathbf{h}_t) = \mathcal{W}(f_t(I; \mathbf{h}_t), \mathbf{t}). \quad (6)$$

Since the calculation of $\arg \max_{\mathbf{t}} \mathcal{W}(f_t(I; \mathbf{h}_t), \mathbf{t})$ is unrelated to \mathcal{W} , we can directly obtain the transformation vector \mathbf{t} from the response map. There is no need to sample the image anymore. Thus, the overall process is highly efficient. The score function f_t can be obtained by

$$f_t(\mathbf{z}) = \mathcal{F}^{-1} \sum_k \hat{\mathbf{h}}_t^{(k)} \odot \hat{\Phi}^{(k)}(\mathbf{z}), \quad (7)$$

where \mathbf{z} indicates a large testing patch. \mathcal{F}^{-1} denotes the inverse Discrete Fourier Transformation operator, \odot is the element-wise multiplication and $\hat{\cdot}$ indicates the Fourier space. $\hat{\mathbf{h}}_t^{(k)}$ and $\hat{\Phi}^{(k)}$ represent the k -th channel of the linear model weights and the feature map, respectively. As

the status space is discrete, it makes the optimization of Eq. 4 to be very efficient. The whole computational cost is $\mathcal{O}(KN \log N)$, where K is the channel number and N is the dimension of the patch \mathbf{z} .

To this end, we need to learn a model \mathbf{h}_t in the process. As in [15], we employ a simple ridge regression learning framework as follows:

$$\left\| \sum_k \Phi^{(k)}(\mathbf{x}) \star \mathbf{h}_t^{(k)} - \mathbf{y} \right\|^2 + \lambda \|\mathbf{h}_t\|_2^2, \quad (8)$$

where \star indicates the correlation operator and λ is the regularization parameter. \mathbf{y} is the desired output, which is typically a Gaussian-like map with maximum value of one. According to Parseval's theorem, the formulation can be calculated without correlation operation. In addition, Eq. 8 can be reformulated as a normal ridge regression by stalling each channel. Thus, the solution to Eq. 8 can be expressed as follows:

$$\hat{\mathbf{h}}_t = (\hat{\mathbf{X}}^T \hat{\mathbf{X}} + \lambda \mathbf{I})^{-1} \hat{\mathbf{X}}^T \hat{\mathbf{y}}, \quad (9)$$

where $\hat{\mathbf{X}} = [\text{diag}(\hat{\Phi}^{(1)}(\mathbf{x}))^T, \dots, \text{diag}(\hat{\Phi}^{(K)}(\mathbf{x}))^T]$ and $\hat{\mathbf{h}}_t = [\hat{\mathbf{h}}_t^{(1)T}, \dots, \hat{\mathbf{h}}_t^{(K)T}]^T$. In this form, we need to solve a $KD \times KD$ linear system, where D is the dimension of testing patch \mathbf{x} .

By applying the kernel trick, the whole system can be simplified as element-wise operation with a linear kernel function $\mathcal{K}(\mathbf{a}, \mathbf{b}) = \mathbf{a}^T \mathbf{b}$. As in [15], the final solution can be derived as below:

$$\begin{aligned} \hat{\mathbf{h}}_t^{(k)} &= \hat{\alpha} \odot \hat{\Psi}^{(k)} \\ &= (\hat{\mathbf{y}} \odot^{-1} (\sum_k \hat{\Phi}^{(k)}(\mathbf{x})^* \odot \hat{\Phi}^{(k)}(\mathbf{x}) + \lambda)) \odot \hat{\Phi}^{(k)}(\mathbf{x})^*, \end{aligned} \quad (10)$$

where α denotes the parameters in dual space and Ψ indicates the model sample in feature space. \odot^{-1} is the element-wise division. Thus, the solution can be

very efficiently obtained with a computational cost of $\mathcal{O}(KD)$. With Eq. 10, the computational cost of Eq. 7 is $\mathcal{O}(KD \log D)$ which is dominated by the FFT operation. For more details, please refer to the seminal work [15, 17].

3.3. Scale and Rotation in Log-polar Coordinates

For correlation filter-based methods, scale changes of the tracked target are usually estimated by sampling the image with different sizes [22, 8]. Therefore, it is quite inefficient to estimate the motion with large displacement. Moreover, it becomes extremely computationally intensive when involving an extra dimension with rotational transformation. To tackle this challenge, we introduce the log-polar coordinates, which is widely used in signal processing to predict the scale and rotation changes.

3.3.1 Log-Polar Coordinates

Suppose an image $I(x, y)$ in the spatial domain, the log-polar coordinates $I'(s, \theta)$ can be viewed as a non-linear and non-uniform transformation of the original Cartesian coordinates. Like polar coordinates, the log-polar coordinates needs a pivot point as the pole and a reference direction as the polar axis in order to expend the coordinates system. One of the dimension is the angle between the point and the polar axis. The other is the logarithm of the distance between the point and the pole.

Given the pivot point (x_0, y_0) and the reference direction \mathbf{r} in Cartesian coordinates, the relationship between Cartesian coordinates and Log-polar coordinates can be formally expressed as follows:

$$\begin{aligned} s &= \log(\sqrt{(x - x_0)^2 + (y - y_0)^2}) \\ \theta &= \cos^{-1}\left(\frac{\langle \mathbf{r}, (x - x_0, y - y_0) \rangle}{\|\mathbf{r}\| \sqrt{(x - x_0)^2 + (y - y_0)^2}}\right). \end{aligned} \quad (11)$$

Usually, the polar axis is chosen as the x -axis in Cartesian coordinates, where θ can be simplified as $\tan^{-1}(\frac{y-y_0}{x-x_0})$. Suppose two images are related purely by rotation $\tilde{\theta}$ and scale $e^{\tilde{s}}$ which can be written as $I_0(e^{\tilde{s}} \cos \theta, e^{\tilde{s}} \sin \theta) = I_1(e^{s+\tilde{s}} \cos(\theta+\tilde{\theta}), e^{s+\tilde{s}} \sin(\theta+\tilde{\theta}))$ in Cartesian coordinates. The log-polar coordinates enjoy an appealing merit that the relationship in the above equation can be derived as the following formula in log-polar coordinates:

$$I'_1(s, \theta) = I'_0(s + \tilde{s}, \theta + \tilde{\theta}), \quad (12)$$

where the pure rotation and scale changes in Log-polar coordinates can be viewed as the translational moving along the axis. As illustrated in Fig. 3, this property naturally can be employed to estimate the scale and rotation changes of the tracked target.

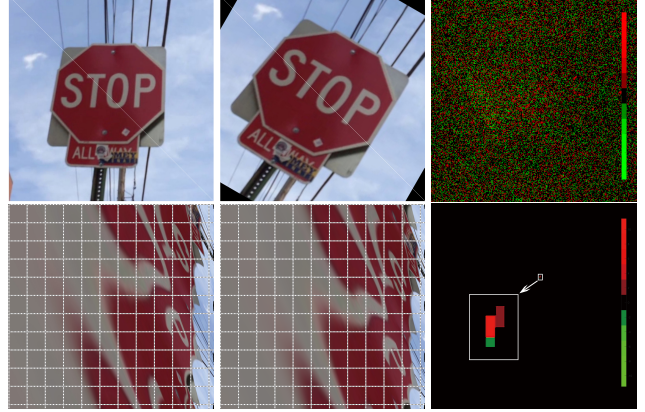


Figure 3: Bottom row is corresponding Log-polar coordinates of the top row. Second column image is a 30° rotation and 1.2 times scale version of the first column. The last column is the phase correlation response maps. In log-polar coordinates, the response is a peak while it is noisy in Cartesian coordinates.

3.3.2 Scale and Rotation Changes

By taking advantage of the log-polar coordinates, Eq. 5 can be calculated very efficiently. Similarly, scale-rotation-invariant can be hold as in Eq. 6. The scale-rotation can be calculated as below:

$$f_\rho(\mathcal{W}(I_i, \rho); \mathbf{h}_\rho) = \mathcal{W}(f_\rho(I_i; \mathbf{h}_\rho), \rho'), \quad (13)$$

where $\rho' = \{\theta', s'\}$ is the coordinates of ρ in log-polar space. $s = e^{s' \log(W/2)/W}$ and $\theta = 2\pi\theta'/H$. H and W is the height and width of the image I_i , respectively. Similar to estimating the translation vector \mathbf{t} by f_t , the whole space of f_ρ can be computed at once through the Fourier trick:

$$f_\rho(\mathbf{z}) = \mathcal{F}^{-1} \sum_k \hat{\mathbf{h}}_\rho^{(k)} \odot \hat{\Phi}^{(k)}(\mathcal{L}(\mathbf{z})), \quad (14)$$

where $\mathcal{L}(x)$ is the log-polar transformation function, and \mathbf{h}_ρ is a linear model weights for scale and rotation estimation. Therefore, the scale and rotation estimation can be obtained very efficiently without any transformation sampling \mathcal{W} . Note that the computational cost of Eq. 14 is unrelated to the sample numbers of scale or rotation. This is extremely efficient compared to the previous enumerate methods [22, 8]

Instead of using the correlation filter-based methods, we employ the phase-correlation to conduct the estimation,

$$\hat{\mathbf{h}}_\rho = \hat{\Upsilon}^* \odot^{-1} |\hat{\Upsilon} \odot \hat{\Phi}(\mathcal{L}(\mathbf{x}))|, \quad (15)$$

where $\Upsilon = \sum_j \beta_j \Phi(\mathcal{L}(\mathbf{x}_j))$ is the linear combination of previous feature patch and $|\cdot|$ is the normal operation. Intuitively, we compute the phase correlation between current frame and the average of previous frames to align the image.

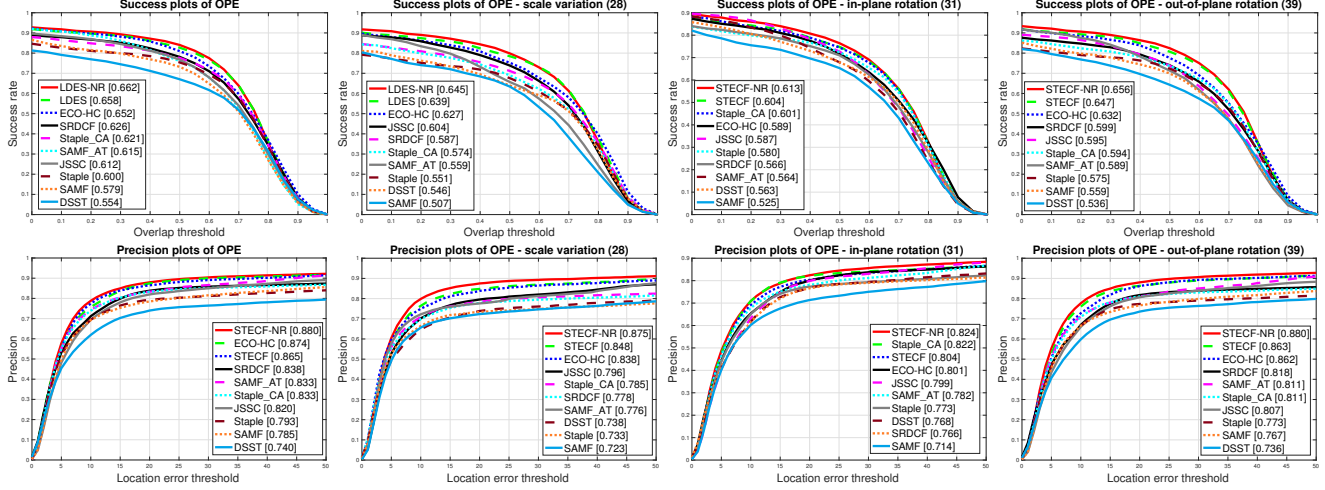


Figure 4: Precision and success plots on OTB-2013 dataset. The first row is the overall performance. Second row shows in-plane rotation performance and the third one is the scale variation performance.

Note that the conventional correlation filter mainly focuses on the center area of the image. It tries to find the similar data structure in the reference frame, which is extremely suitable for the translation estimation. However, the entire image is full of the tracked target in predicting scale and rotation changes. Focusing on the center may lead to the unstable matching results. On the contrary, the phase correlation is quite effective to deal with this issue.

3.4. Implementation Details

In this work, we alternatively optimize Eq. 4 and Eq. 5 until $f(\mathbf{x})$ does not decrease or reaches the maximal number of iterations. After the optimization, we update the correlation filter model as in [15],

$$\hat{\Psi}_i = (1 - \lambda_\phi)\hat{\Psi}_{i-1} + \lambda_\phi\hat{\Phi}(\mathbf{x}_i), \quad (16)$$

where λ_ϕ is the update rate of the feature data model in Eq. 10. The kernel weight in dual space is updated as below:

$$\hat{\alpha}_i = (1 - \lambda_\alpha)\hat{\alpha}_{i-1} + \lambda_\alpha(\hat{\mathbf{y}} \odot^{-1} \left(\sum_k \hat{\Phi}^{(k)}(\mathbf{x}_i) * \hat{\Phi}^{(k)}(\mathbf{x}_i) + \lambda \right)), \quad (17)$$

where λ_α is the update of the kernel parameter in dual space of Eq. 10. Although there exist some theoretical sounding updating schemes [18, 7, 9], the reason we use linear combination is due to its efficiency and the comparable performance.

Meanwhile, we also update the scale and rotation model as a linear combination,

$$\Upsilon_i = (1 - \lambda_w)\Upsilon_{i-1} + \lambda_w\Phi(\mathcal{L}(\mathbf{x}_i)), \quad (18)$$

where λ_w can be explained as an exponentially weighted average of the model $\beta_j\Phi(\mathcal{L}(\mathbf{x}_j))$. We update the model

upon Φ instead of x_i because $\Phi(\sum_i \mathcal{L}(\mathbf{x}_i))$ is not defined. It intends to blur the image due to the logarithm function in which decreases the visual feature information.

As the image patch \mathbf{x} is discrete, the status \mathbf{t} and ρ estimated by $f_t(\mathbf{x})$ and $f_\rho(\mathbf{x})$ are also discrete. This causes artificial effects in status estimation since the changes between the frames is usually very tiny. To this end, we interpolate the f_t and f_ρ with a centroid-based method to obtain sub-pixel level precision.

In addition, unlike conventional correlation filter-based method, the size of \mathbf{z} in testing and \mathbf{x} in training time are different, since the patch size of \mathbf{z} in Eq. 7 is actually the search size of the correlation filter method. A larger search range ($N > D$) helps to reduce the searching time and also improve the robustness for the solution to sub-problems. To match the different dimension N and D , we padding \mathbf{h} with zero in spatial space. All patch is multiplied a Hann window as suggested in [5].

4. Experiments

4.1. Experimental Settings

We evaluate our proposed Similarity Transformation Estimation for Correlation Filter tracker (STECF) in two different testbeds. OTB-2013 [35] contains 51 sequences which are commonly used in generic object tracking community. One of its objectives is to test the generality of the trackers. Thus, only the axis-aligned bounding box is labeled, which is insufficient to evaluate the in-plane rotation accuracy. To better evaluate our proposed method, Planar Object Tracking (POT) benchmark [23] is employed to examine the performance on 2D similarity transformation estimation. It is important to note that POT is designed to evaluate the planar object tracking method with strong ho-

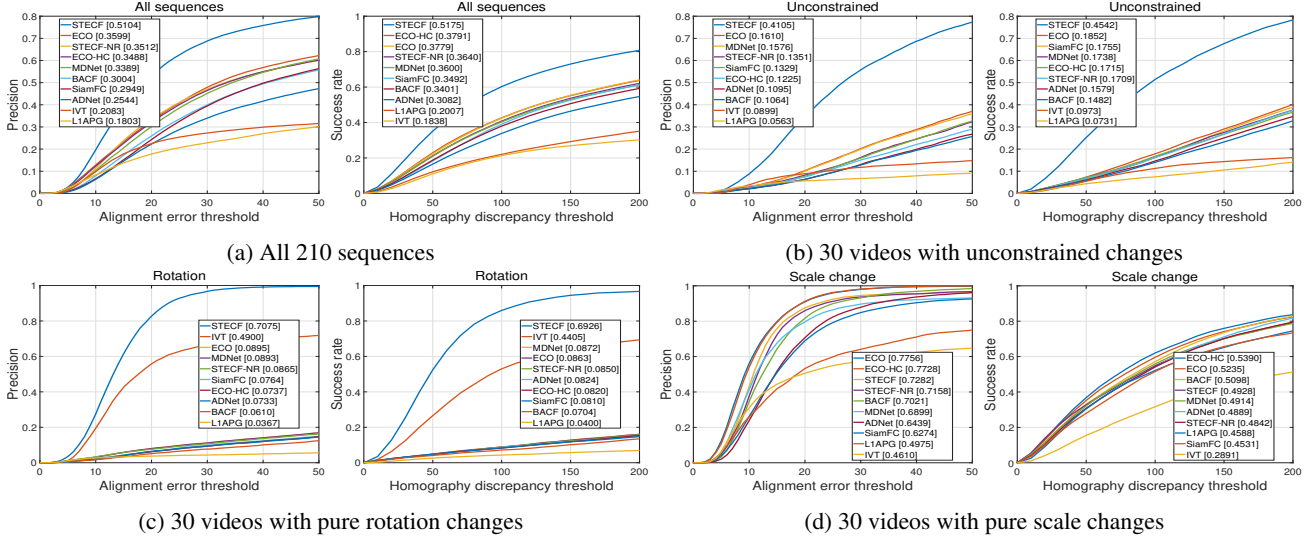


Figure 5: Precision and success plots on the POT dataset.

mography assumption. We also implement a No-Rotation version of our method, STECF-NR, which is used to better demonstrate our proposed method. All the methods are implemented in Matlab. All the experiments are conducted on a PC with an Intel i7-4770 3.40GHz CPU and 16GB RAM. The average running time of our proposed STECF and STECF-NR is around 22fps and 140fps, respectively.

We employ HoG feature for both translational and scale-rotation estimation, and the extra color histogram is used to estimate translational. η is 0.15 and λ is set to $1e^{-4}$. λ_ϕ and λ_α are both set to 0.01. λ_ω is 0.015. For translational estimation, the size of learning patch D is 2.5 larger than the original target size. Moreover, the searching window size N is about 1.5 larger than the learning patch size D . For scale-rotation estimation, the phase correlation sample size is about 1.8 larger than the original target size. All parameters are fixed in the following experiments. We will release the source code to reproduce our experimental results.

4.2. Comparison with Correlation Filter Trackers

We first evaluate our proposed tracker on OTB-2013 dataset [35] with the default setting. To facilitate fair comparison, we select eight state-of-the-art Correlation Filter-based trackers without deep learning features as reference methods, including ECO-HC [7], SRDCF [9], Staple [2], SAMF [22], DSST [8], JSSC [38], Staple_CA [25], and SAMF_AT [4].

Fig. 4 shows the experimental results of the overall sequences, the sequences with in/out-plane rotations and the sequences of scale variations. It can be clearly seen that both STECF and STECF-NR obtain 65.8% and 66.2% in success plot respectively, which is better than other correlation filter-based trackers, e.g. 65.2% for ECO-HC and

62.6% for SRDCF. In the scale variation success plot, our proposed trackers achieves 64.5% and 63.9% comparing to ensemble-based scale estimator like SAMF (50.7%) and DSST (54.6%), which accounts for a large performance boost over 10%. Moreover, our implementation is also better than the 62.1% for Staple_CA and 61.5% for SAMF_AT, which are two improved version of original trackers proposed recently. This demonstrates that our proposed methods have superior scale estimation performance over the ensemble-based scale estimation approaches.

In rotation attributed plots, STECF performs 60.4% and 64.7% in in/out-plane attributed success plots. Our results are better than the similarity estimation-enabled tracker JSSC, which achieves 58.7% in in-plane rotation attributed success plot, and 59.5% in out-of-plane rotation attributed plot, respectively. This demonstrates that our rotation estimation is more robust in different sequences.

Please note that our proposed STECF is quite stable in searching the 4-DoF status space, since the performance only drops 0.4% from 66.2% to 65.8% in overlap metric, and 0.6% in overall location error metric. We argue that the reason why STECF-NR outperform STECF in rotation plot is due to the lack of ground truth on rotation in the OTB-2013 benchmark. This limits the evaluation performance of our proposed STECF. Fig. 6 demonstrates several sample results on various videos [36, 23]. (The video sequences of tracking result are provided in supplementary materials)

4.3. Comparison with State-of-the-Art trackers

To better evaluate our proposed STECF approach on rotation estimation, we conduct additional experiment on POT benchmark [23]. The POT dataset contains 30 objects with 7 different categories which yield 210 videos in to-

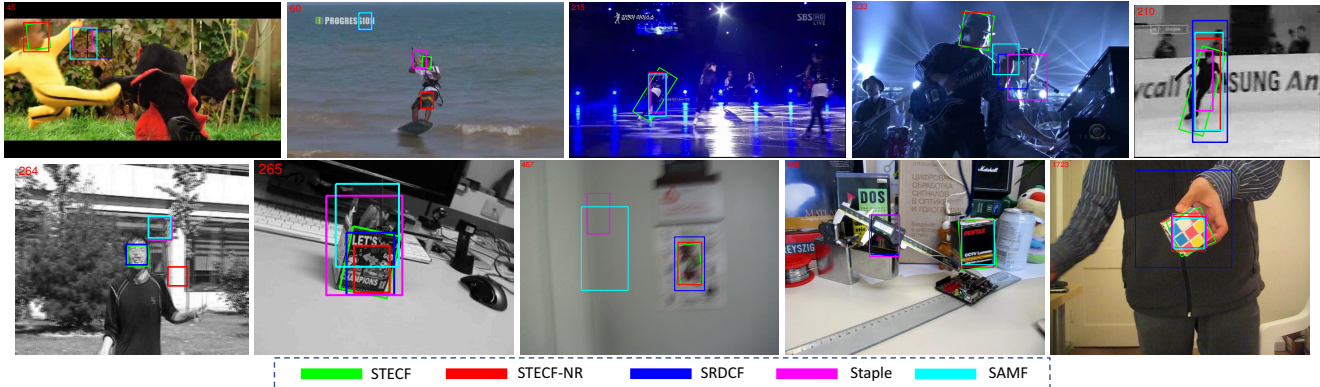


Figure 6: Sample video results with different trackers.

	ECO	MDNet	BACF	ADNet	STECF
ALL	0.3599	0.3389	0.3004	0.2544	0.5104
SC	0.7756	0.6899	0.7021	0.6439	0.7282
RT	0.0895	0.0893	0.0610	0.0733	0.7075
PD	0.2359	0.2614	0.1961	0.1832	0.2784
MB	0.1540	0.1412	0.1155	0.0829	0.1748
OCC	0.5610	0.5307	0.4695	0.4723	0.6991
OV	0.5421	0.5021	0.4520	0.2158	0.5743
UC	0.1610	0.1576	0.1064	0.1095	0.4105

Table 2: Comparison in all 7 categories attributed videos

tal. All sequences are labeled with homography transformation using four-corner points. Alignment error and homography discrepancy are employed as the evaluation metrics. As in [23], alignment error is the average distance error between four ground truth points and tracker’s output. Homography discrepancy denotes the distance between the two homography matrices. In addition, six state-of-the-art trackers and two rotation-enabled trackers are involved to demonstrate the significance and generality of our proposed work. They are ECO-HC, ECO [7], MDNet [26], BACF [12], ADNet [37], SiameseFC [3], IVT [31] and L1APG [16]. To illustrate the POT plots appropriately, we set the maximal value of the alignment error axis from 20 to 50 pixels in precision plot and utilize the AUC as the metrics for ranking in both precision and homography discrepancy plots as same as OTB-2013 [35].

Fig. 5 shows the results different attributed plots. Our proposed STECF tracker, with hand-craft features only, performs extremely well in all sequences attributed plots and even outperforms deep learning based methods with a large margin. This demonstrates the significance of the similarity-enabled representation in tracking task. Moreover, our rotation-disabled version of tracker, STECF-NR, outperforms MDNet which is considered as state-of-the-art pure deep learning tracker. Since the POT sequences are quite different from OTB benchmark, it indicates our proposed method has better generalization capabilities compared with pure deep learning based approaches in wide

scenarios. This demonstrates that our proposed method is able to search the 4-DoF similarity transformation status simultaneously, efficiently and precisely.

In Rotation attributed plots, IVT performs fairly well compared to its results in other plots. STECF still outperforms IVT over 20% in both precision and homography plots. It not only proves the effectiveness of our proposed rotation estimation but also shows the superiority of our method compared with traditional approaches. It is quite surprising that L1APG does not work with rotation changes in our experiments. Meanwhile, STECF achieves 41.05% and 45.42% compared with second ranked 16.1% and 18.52% of ECO in Unconstrained plots, in which various changes in the video, e.g. motion blur, occlusions and out of view. Our rotation-enabled proposed STECF tracker are more capable in wide scenarios.

In Scale change attributed plots, all trackers achieve much better scores compared with their performance in other plots. Our proposed STECF ranks 3rd and 4th and is comparable with BACF. However, as shown in Table 2, our proposed tracker outperforms others in 6 out of 7 categories. We argue that all recent proposed trackers are quite comparable to each other in pure scale changes because their output cannot fix into projective transformation, which is used in POT.

5. Conclusion

In this paper, we proposed a novel visual object tracker for robust estimation of similarity transformation with correlation filter. We formulated the 4-DoF searching problem into two 2-DoF sub-problems and applied a Block Coordinates Descent solver to search in such a large 4-DoF space in real-time. Specifically, we employed an efficient phase correlation scheme to deal with both scale and rotation changes simultaneously in log-polar coordinates and utilized a fast variant of correlation filter to predict the translational motion. Experimental results demonstrated that the proposed tracker achieves very promising prediction per-

formance compared with the state-of-the-art visual object tracking methods. Moreover, as a fundamental approach in estimation of similarity transformation, our proposed method can be further improved by combining with deep learning features and other state-of-the-art approaches.

References

- [1] S. Baker and I. Matthews. Lucas-kanade 20 years on: A unifying framework. *IJCV*, 56(3):221–255, 2004. 2
- [2] L. Bertinetto, J. Valmadre, S. Golodetz, O. Miksik, and P. Torr. Staple: Complementary learners for real-time tracking. In *CVPR*, 2015. 2, 7
- [3] L. Bertinetto, J. Valmadre, J. Henriques, A. Vedaldi, and P. H. Torr. Fully-convolutional siamese networks for object tracking. *ECCV Workshop*, 2016. 2, 3, 8
- [4] A. Bibi, M. Mueller, , and B. Ghanem. Target response adaptation for correlation filter tracking. In *ECCV*, 2016. 7
- [5] D. S. Bolme, J. R. Beveridge, B. A. Draper, and Y. M. Lui. Visual object tracking using adaptive correlation filters. In *CVPR*, 2010. 2, 6
- [6] E. D. Castro and C. Morandi. Registration of translated and rotated images using finite fourier transforms. *TPAMI*, 9(5):700–703, 1987. 3
- [7] M. Danelljan, G. Bhat, F. Khan, and M. Felsberg. Eco: Efficient convolution operators for tracking. In *CVPR*, 2017. 1, 2, 3, 6, 7, 8
- [8] M. Danelljan, G. Häger, F. Khan, and M. Felsberg. Discriminative scale space tracking. *TPAMI*, 2017. 2, 5, 7
- [9] M. Danelljan, G. Hger, F. Khan, and M. Felsberg. Learning spatially regularized correlation filters for visual tracking. In *ICCV*, 2015. 1, 2, 6, 7
- [10] M. Danelljan, A. Robinson, F. Khan, and M. Felsberg. Beyond correlation filters: Learning continuous convolution operators for visual tracking. In *ECCV*, 2016. 1, 3
- [11] A. Doucet, N. de Freitas, and N. Gordon. *Sequential Monte Carlo Methods in Practice*. Springer-Verlag, 2001, 2001. 3
- [12] H. K. Galoogahi, A. Fagg, and S. Lucey. Learning background-aware correlation filters for visual tracking. In *ICCV*, 2017. 1, 2, 8
- [13] Q. Guo, W. Feng, C. Zhou, R. Huang, L. Wan, and S. Wang. Learning dynamic siamese network for visual object tracking. In *ICCV*, 2017. 3
- [14] D. Held, S. Thrun, and S. Savarese. Learning to track at 100 fps with deep regression networks. In *ECCV*, 2016. 1
- [15] J. Henriques, R. Caseiro, P. Martins, and J. Batista. High-speed tracking with kernelized correlation filters. In *IEEE TPAMI*, volume 37, pages 583–596, 2015. 1, 2, 4, 5, 6
- [16] H. Ji. Real time robust l1 tracker using accelerated proximal gradient approach. In *CVPR*, pages 1830–1837, 2012. 2, 8
- [17] H. Kiani, T. Sim, and S. Lucey. Multi-channel correlation filters. In *ICCV*, 2013. 4, 5
- [18] H. Kiani, T. Sim, and S. Lucey. Correlation filters with limited boundaries. In *CVPR*, 2015. 1, 6
- [19] M. Kristan, J. Matas, A. Leonardis, M. Felsberg, L. Cehovin, G. Fernandez, T. Vojir, G. Hager, G. Nebehay, and R. Pflugfelder. The visual object tracking vot2015 challenge results. In *ICCV Workshops*, 2015. 2
- [20] H. Li, Y. Li, and F. Porikli. Deeptack: Learning discriminative feature representations online for robust visual tracking. *TIP*, 25(4):1834–1848, 2016. 1
- [21] Y. Li and G. Liu. Learning a scale-and-rotation correlation filters for robust visual tracking. In *ICIP*, 2016. 3
- [22] Y. Li and J. Zhu. A scale adaptive kernel correlation filter tracker with feature integration. In *ECCV Workshops*, 2014. 2, 5, 7
- [23] P. Liang, Y. Wu, and H. Ling. Planar object tracking in the wild: A benchmark. *CoRR*, abs/1703.07938, 2017. 6, 7, 8
- [24] D. G. Lowe. Distinctive image features from scale-invariant keypoints. *IJCV*, 60(2):91–110, Nov 2004. 2
- [25] M. Mueller, N. Smith, and B. Ghanem. Context-aware correlation filter tracking. In *CVPR*, 2017. 1, 3, 7
- [26] H. Nam and B. Han. Learning multi-domain convolutional neural networks for visual tracking. In *CVPR*, 2016. 1, 2, 3, 8
- [27] G. Nebehay and R. Pflugfelder. Consensus-based matching and tracking of keypoints. In *Winter Conference on Applications of Computer Visio*, 2014. 2
- [28] Y. Nesterov. Efficiency of coordinate descent methods on huge-scale optimization problems. *SIAM Journal on Optimization*, 22(2):341–362, 2010. 4
- [29] G. Ravichandran and D. Casasent. Advanced in-plane rotation-invariant correlation filters. *TPAMI*, 16(4):415–420, 1994. 3
- [30] P. Richtárik and M. Takáč. Iteration complexity of randomized block-coordinate descent methods for minimizing a composite function. *Mathematical Programming*, 144(1):1–38, Apr 2014. 4
- [31] D. A. Ross, J. Lim, R.-S. Lin, and M.-H. Yang. Incremental learning for robust visual tracking. *IJCV*, 77(1-3):125–141, 2008. 2, 8
- [32] W. Song, J. Zhu, Y. Li, and C. Chen. Image alignment by online robust pca via stochastic gradient descent. *IEEE Transactions on Circuits and Systems for Video Technology*, 26(7):1241–1250, July 2016. 2
- [33] Y. Song, C. Ma, L. Gong, J. Zhang, R. Lau, and M.-H. Yang. Crest: Convolutional residual learning for visual tracking. In *ICCV*, 2017. 3
- [34] J. Valmadre, L. Bertinetto, J. F. Henriques, A. Vedaldi, and P. H. Torr. End-to-end representation learning for correlation filter based tracking. In *CVPR*, 2017. 3
- [35] Y. Wu, J. Lim, and M.-H. Yang. Online object tracking: A benchmark. In *CVPR*, 2013. 6, 7, 8
- [36] Y. Wu, J. Lim, and M.-H. Yang. Object tracking benchmark. *TPAMI*, 37(9):1834–1848, 2015. 7
- [37] S. Yun, J. Choi, Y. Yoo, K. Yun, and J. Y. Choi. Action-decision networks for visual tracking with deep reinforcement learning. In *CVPR*, 2017. 3, 8
- [38] M. Zhang, J. Xing, J. Gao, X. Shi, Q. Wang, and W. Hu. Joint scale-spatial correlation tracking with adaptive rotation estimation. In *ICCV Workshop*, 2015. 3, 7
- [39] T. Zhang, C. Xu, and M.-H. Yang. Multi-task correlation particle filter for robust object tracking. In *CVPR*, 2017. 2
- [40] S. Zokai and G. Wolberg. Image registration using log-polar mappings for recovery of large-scale similarity and projective transformations. *TIP*, 14(10):1422–1434, 2005. 3

- [41] M. Zuysal, M. Calonder, V. Lepetit, and P. Fua. Fast keypoint recognition using random ferns. *TPAMI*, 32(3):448, 2010. 2